

Article

Pt₂CeO₂ Heterojunction Supported on Multiwalled Carbon Nanotubes for Robust Electrocatalytic Oxidation of Methanol

Pingping Yang^{1,2} , Xuejiao Wei^{1,*}, Li Zhang¹, Shiming Dong¹, Wenting Cao¹, Dong Ma¹ and Yuejun Ouyang^{1,2,*}

¹ College of Chemistry and Materials Engineering, Huaihua University, Huaihua 418008, China

² Hunan Engineering Research Center for Recycled Aluminum, Huaihua University, Huaihua 418008, China

* Correspondence: weil348137@163.com (X.W.); oyyj0816@163.com (Y.O.)

Abstract: Herein, we prepared Pt₂CeO₂ heterojunction nanocluster (HJNS) on multiwalled carbon nanotubes (MWCNTs) in deep eutectic solvents (DESs) which is a special class of ionic liquids. The catalyst was then heat-treated at 400 °C in N₂ (refer to Pt₂CeO₂/CNTs-400). The Pt₂CeO₂/CNTs-400 catalyst showed remarkably improved electrocatalytic performance towards methanol oxidation reaction (MOR) (839.1 mA mg_{Pt}⁻¹) compared to Pt₂CeO₂/CNTs-500 (620.3 mA mg_{Pt}⁻¹), Pt₂CeO₂/CNTs-300 (459.2 mA mg_{Pt}⁻¹), Pt₂CeO₂/CNTs (641.6 mA mg_{Pt}⁻¹) (the catalyst which has not been heat-treated) and commercial Pt/C (229.9 mA mg_{Pt}⁻¹). Additionally, the Pt₂CeO₂/CNTs-400 catalyst also showed better CO poisoning resistance (onset potential: 0.47 V) compared to Pt₂CeO₂/CNTs (0.56 V) and commercial Pt/C (0.58 V). The improved performance of Pt₂CeO₂/CNTs-400 catalyst is attributed to the addition of appropriate CeO₂, which changed the electronic state around the Pt atoms, lowered the d-band of Pt atoms, formed more Ce-O-Pt bonds acting as new active sites, affected the adsorption of toxic intermediates and weakened the dissolution of Pt; on the other hand, with the assistance of thermal treatment at 400 °C, the obtained Pt₂CeO₂ HJNS expose more new active sites at the interface between Pt and CeO₂ to enhance the electrochemical active surface area (ECSA) and the dehydrogenation process of MOR. Thirdly, DES is beneficial to the increase of the effective component Pt(0) in the carbonization process. The study shows a new way to construct high-performance Pt-CeO₂ catalyst for the direct methanol fuel cell (DMFC).

Keywords: Pt₂CeO₂ heterojunction nanocluster; Ce-O-Pt bonds; methanol oxidation reaction; deep eutectic solvents; direct methanol fuel cell



Citation: Yang, P.; Wei, X.; Zhang, L.; Dong, S.; Cao, W.; Ma, D.; Ouyang, Y. Pt₂CeO₂ Heterojunction Supported on Multiwalled Carbon Nanotubes for Robust Electrocatalytic Oxidation of Methanol. *Molecules* **2023**, *28*, 2995. <https://doi.org/10.3390/molecules28072995>

Academic Editors: Zhijian Tan, Hongye Cheng and Baokun Tang

Received: 31 December 2022

Revised: 19 March 2023

Accepted: 20 March 2023

Published: 27 March 2023



Copyright: © 2023 by the authors. Licensee MDPI, Basel, Switzerland. This article is an open access article distributed under the terms and conditions of the Creative Commons Attribution (CC BY) license (<https://creativecommons.org/licenses/by/4.0/>).

1. Introduction

The development of fuel cells is one of the important ways to achieve carbon neutrality [1–4]. Fuel cells have been the focus of attention in the field of energy, such as direct methanol fuel cells (DMFCs) [5,6], direct ethanol fuel cells (DEFCs) [7], direct formic acid fuel cells (DFAFCs) [8] and so on. Among them, with the advantages of easy operation, safe liquid methanol, high energy density and low operating temperature, DMFCs have received extensive attention as a hopeful power technology for vehicles and portable electronic devices [9,10].

As we know, the precious metal platinum (Pt) has excellent catalytic performance for the DMFC. However, the high price and scarcity of Pt hinder the commercialization of these technologies. Additionally, Pt-based catalysts are susceptible to poisoning by carbonaceous intermediates (mainly CO_{ads}) that are adsorbed on the Pt active sites and reduce the catalytic performance towards MOR. According to the bifunctional mechanism, in order to effectively alleviate the toxicity of CO_{ads} to the Pt active site, introducing a second cheap metal is an effective method. Due to the effect of the added metal on the electronic structure, the Pt electronic state is changed to reduce the adsorption of poisonous intermediates (e.g., CO_{ads}, COOH_{ads}). Among these alloy catalysts, the Pt-CeO₂ binary

system has attracted much interest [11–13]. Herein, ceria nanorods with rich oxygen vacancies and rough surface have been induced by plasma surface engineering and used as Pt support. The prepared Pt/CeO₂-P catalyst shows enhanced mass activity towards MOR [14]. In addition, Pt-CeO₂/C-S catalyst with CeO₂ nanospheres as initiator has the highest catalytic performance for MOR, which is due to the physical interaction and electronic effect between CeO₂ and Pt [15]. In addition, carbon-free PtCu/CeO₂ catalyst was prepared by Cu pre-coating CeO₂. The mass activity of PtCu/CeO₂ catalysts for MOR and oxygen reduction (ORR) was 1.84 and 1.57 times that of Pt/C, respectively [16]. At present, Pt-CeO₂ system catalysts have been studied extensively. How to further improve the catalytic activity of the catalyst and apply it to actual direct methanol fuel cells is the direction of the researchers' efforts.

Pt-based nanoparticles supported on carbon black (e.g., Vulcan XC-72) nanocatalysts are commonly used in the DMFC [17]. However, the deep micropores or recesses of carbon black nanocatalysts limit their use as a catalyst support because the catalytic nanoparticles get trapped in the micropores and become electrochemically inaccessible [18]. Another promising carbon material such as graphene-like carbon nitride can be used in many fields (e.g., photo-degradation intermediates). Xia et al. prepared Fe-ZrO₂ embedding g-C₃N₄ by solvothermal method for photo-degradation of anti-diabetic drug, acarbose (ACB) [19]. Graphene has made great progress as a catalyst carrier. However, the conductivity of graphene-based carbon materials needs to be improved. Another carbon material could solve the problem graphene could not solve in terms of electron transport. Multiwalled carbon nanotubes (MWCNTs) have unique morphologies and properties, such as high specific surface area and corrosion resistance, good electronic conductivity and high stability [20–22]. In addition, MWCNTs heterojunction with graphene-like carbon nitride can enhance the electrochemical and photocatalytic activity. For example, Tahir Muhmood et al. reported electro-static junctions between carbon nanotubes (CNT) and graphitic carbon nitride (CCN) with enhanced photocatalytic properties [23]. Although MWCNTs have these advantages, pristine MWCNTs lack sufficient binding sites and are chemically inert for anchoring metal nanoparticles which results in poor dispersion and aggregation. Therefore, we introduced the above CeO₂-modified MWCNTs to support nanoparticles more stably [24].

Through interface engineering to construct a heterojunction catalyst, its unique advantage can effectively improve the catalytic activity compared with one component catalyst. Synergistic effects are common in heterojunction catalysts, both electronic interactions and defect effects in heterojunction are conducive to improving catalytic activity [25]. For example, Xia et al. reported a novel type-I heterojunction between red phosphorus and graphitic carbon nitride under vacuum condition. The red phosphorus/graphitic carbon nitride possess type-I heterojunction with enhanced catalytic behavior [26]. Tahir Muhmood et al. used the vacuum tube method to construct nondestructive and physically stable graphitic carbon nitride/graphene nanoplatelet composites, which achieved the complete degradation of tetracycline hydrochloride [27]. It can be seen that the construction of heterojunction catalyst has the potential to improve the catalytic performance.

Deep eutectic solvents (DESs) are a new kind of ionic liquids consisting of quaternary ammonium salts and hydrogen bond donors [28–34]. Abbott et al. reported these green solvents firstly have received intensive attention in electrocatalysis applications due to their remarkable physicochemical properties (high conductivity, thermostability, negligible vapor pressure and wide electrochemical potential windows) [35]. Recently, Hsieh et al. prepared sc-Pd NPs/GR/SPCE (screen-printed carbon electrode) which shows excellent activity towards glycerol oxidation compared to composites not fabricated by sc CO₂ processes [36]. Palomar-Pardavé et al. prepared Pd@Pd(OH)₂ core-shell nanoparticles in DES. It is shown that the GCE (glassy carbon electrode)/Pd@Pd(OH)₂-modified electrode displays a high catalytic activity towards the MOR in alkaline solution [37]. Fan et al. have prepared high-performance Pt-based alloy catalysts by chemical reduction or electrochemistry method in DES that plays an important role in controlling the shape of the

nanoparticles [38,39]. In our previous work, a series of Pt/Pd-based catalysts have been prepared using DES [21,24,40,41]. DES has been widely proved to be a green solvent for the preparation of high-performance catalysts. Therefore, DES is expected to be further widely used in more fields.

Herein, we fabricated Pt₂CeO₂ HJNS supported on MWCNTs catalyst successfully with the help of DES and the pyrolysis process. The related results demonstrated that we used the combination of (Pt + CeO₂ + MWCNTs + DES + calcination) to get a material with rich structure, so as to obtain good MOR catalytic performance. The prepared Pt₂CeO₂/CNTs-400 exhibits enhanced catalytic activity and stability for the MOR compared with Pt₂CeO₂/CNTs-500, Pt₂CeO₂/CNTs-300, Pt₂CeO₂/CNTs and Pt/C catalysts.

2. Results and Discussion

Figure 1 shows the XRD patterns of Pt₂CeO₂/CNTs and Pt₂CeO₂/CNTs-400 catalysts. The peak at approximately 26.2° for both catalysts was due to the (002) crystal phase of the MWCNTs [42]. The two catalysts show peaks characteristic of Pt, that is, 40.8°, 47.8°, 68.5°, 82.9° and 87.3° of (111), (200), (220), (311) and (222), respectively [38]. Four diffraction peaks (111), (200), (311) and (420) of CeO₂ were observed in Pt₂CeO₂/CNTs-400 corresponding to 28.5°, 33°, 56.7° and 79°, respectively [24]. Interestingly, the diffraction peaks of CeO₂ (220) are combined with Pt(200) approximately at 2θ = 47.8°. It is worth noting that the peak of CeO₂ (311) appeared strongly in the non-pyrolytic Pt₂CeO₂/CNTs material, while after 400 °C heat treatment, the peaks of CeO₂ (311) disappeared and CeO₂ (111) and CeO₂ (200) appeared in the Pt₂CeO₂/CNT-400. This result indicates that proper pyrolysis is conducive to the formation of different crystalline of CeO₂, and these CeO₂ distributed in different places can promote the catalytic effect of Pt better.

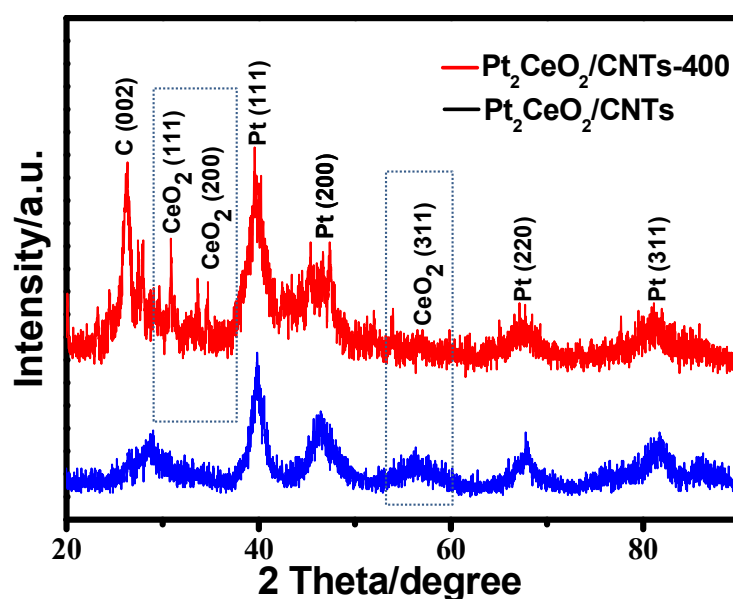


Figure 1. XRD patterns of Pt₂CeO₂/CNTs and Pt₂CeO₂/CNTs-400 catalysts.

Figure S1 from Supplementary Materials shows the XRD patterns of Pt₂CeO₂/CNTs-300 and Pt₂CeO₂/CNTs-500 catalysts. The average crystallite size of the Pt nanoparticles was determined to be 4.5 ± 1.14, 4.5 ± 1.06, 4.3 ± 1.07 and 4.4 ± 1.11 nm for the Pt₂CeO₂/CNTs-400, Pt₂CeO₂/CNTs-300, Pt₂CeO₂/CNTs-500 and Pt₂CeO₂/CNTs, respectively, calculated from the Pt(220) diffraction peak using Scherrer's equation [43–45]. The result shows that pyrolysis has no significant effect on particle size for all catalysts.

Figure 2 shows the TEM and HRTEM images, HAADF-STEM elements mapping and the corresponding elements Pt, Ce and O of Pt₂CeO₂/CNTs-400. As shown in Figure 2a,b, the Pt₂CeO₂ HJNS are evenly dispersed on MWCNTs with no aggregation. The average size of Pt nanoparticles in the Pt₂CeO₂/CNTs-400 is approximately 4.5 ± 1.14 nm, which is very

close to the XRD data above. The HRTEM image of $\text{Pt}_2\text{CeO}_2/\text{CNTs-400}$ (Figure 2c) shows the crystal plane distances of 0.312 nm obtained for the CeO_2 (111) plane and 0.225 nm for the Pt(111) plane; both agree very well with the known crystal plane distances [24]. In addition, as shown in Figure S2 from Supplementary Materials, the Pt nanoparticles are also dispersed well with no aggregation and the average particle size is approximately 4.4 ± 1.11 nm of $\text{Pt}_2\text{CeO}_2/\text{CNTs}$. Figure S3 from Supplementary Materials shows the TEM and HRTEM images of $\text{Pt}_2\text{CeO}_2/\text{CNTs-300}$ and $\text{Pt}_2\text{CeO}_2/\text{CNTs-500}$ catalysts. We can see that these catalysts $\text{Pt}_2\text{CeO}_2/\text{CNTs-400}$, $\text{Pt}_2\text{CeO}_2/\text{CNTs-300}$, $\text{Pt}_2\text{CeO}_2/\text{CNTs-500}$ and $\text{Pt}_2\text{CeO}_2/\text{CNTs}$ which were fabricated in DES probably act as a kind of surfactants, additives, or stabilizers to induce a uniform distribution for Pt and CeO_2 nanoparticles. However, systematic studies aimed at understanding the role of DES in the prepared process are still underway. EDX spectrum (Figure S4 from Supplementary Materials) of the $\text{Pt}_2\text{CeO}_2/\text{CNTs-400}$ catalyst displays the signals of C, O, Pt and Ce elements, confirming the pyrolysis does not affect the metal composition in the catalyst.

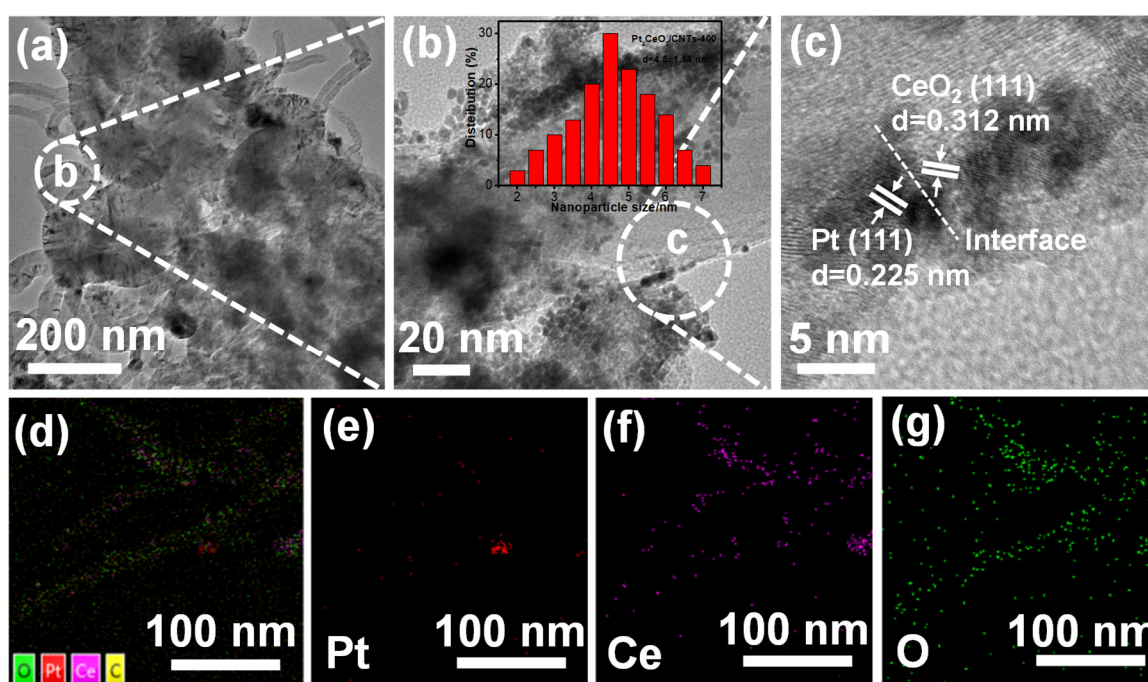


Figure 2. (a) TEM and (b,c) HRTEM images; the corresponding particle size distribution of $\text{Pt}_2\text{CeO}_2/\text{CNTs-400}$; (d–g) HAADF-STEM elements mapping; the corresponding elements Pt, Co and O of $\text{Pt}_2\text{CeO}_2/\text{CNTs-400}$.

The surface composition and chemical oxidation states of these catalysts were characterized by XPS. Figure 3a shows the XPS survey spectra of $\text{Pt}_2\text{CeO}_2/\text{CNTs-400}$ and $\text{Pt}_2\text{CeO}_2/\text{CNTs}$. The signals corresponding to C 1s (283.8 eV), O 1s (531.9 eV), Ce 3d (~900.8 eV), Pt 4f (73.4 eV) and Pt 4d (315.1 eV) were observed for these two catalysts. Figure 3b shows the Ce3d spectrum of $\text{Pt}_2\text{-CeO}_2/\text{CNTs-400}$; the deconvolution of the asymmetric Ce3d photoemission of the $\text{Pt}_2\text{CeO}_2/\text{CNTs-400}$ produced four peaks at 881.8, 885.1, 900.5 and 903.8 eV. To further determine the presence of Ce3d peaks, we locally enlarged the peak shape of Ce3d in Figure S5 from Supplementary Materials. From the enlarged figure, it can be seen that the Ce3d peaks of the two catalysts do exist, but the peaks are small, which may be attributed to the small content of Ce. Figure 3c,d show the Pt 4f spectra for $\text{Pt}_2\text{CeO}_2/\text{CNTs}$ and $\text{Pt}_2\text{CeO}_2/\text{CNTs-400}$ catalysts. The Pt 4f spectra of the $\text{Pt}_2\text{CeO}_2/\text{CNTs}$, two pairs of peaks, indicate the existence of two different Pt oxidation states on the surface, and two intense peaks located at binding energies of 70.7 eV (Pt 4f 7/2) and 74.1 eV (Pt 4f 5/2) originated from metallic Pt(0), and the weak peaks located at 71.5 eV (Pt 4f 7/2) and 74.4 eV (Pt 4f 5/2) were assigned to the Pt(II) state in the form

of PtO or Pt(OH)₂ [46]. For the Pt₂CeO₂/CNTs-400 catalyst, the Pt 4f 7/2 peak located at 71.0 eV and Pt 4f 5/2 peak located at 74.4 eV correspond to metallic Pt(0), and the Pt 4f 7/2 peak located at 71.8 eV and Pt 4f 5/2 peak located at 75.3 eV correspond to Pt(II) in PtO or Pt(OH)₂. The fractions of the Pt(0) and Pt(II) species in Pt₂CeO₂/CNTs-400 and Pt₂CeO₂/CNTs were calculated as (40.3%, 59.7%) and (46.2%, 53.8%), respectively. The content of Pt(0) in Pt₂CeO₂/CNTs-400 is higher than that in Pt₂CeO₂/CNTs, which is also due to the carbonization of DES in the pyrolysis process [47]. In addition, the positive shift (about 0.3 eV) in the Pt peaks was observed in the Pt₂CeO₂/CNTs-400, which indicates the interaction of CeO₂ and Pt, exposing the strong electronic interactions between CeO₂ and Pt nanoparticles by the formation of Ce-O-Pt [24]. The electronic interaction between CeO₂ and Pt nanoparticles can alter the electronic environment of Pt atoms, thus affecting the bonding between Pt and intermediates (such as CO_{ads}). Thus, the electrocatalytic performance of MOR was improved. Figure S6 from Supplementary Materials shows the Pt 4f and Ce 3d spectra for Pt₂CeO₂/CNTs-300 and Pt₂CeO₂/CNTs-500 catalysts. For the Pt₂CeO₂/CNTs-300 catalyst, the Pt 4f 7/2 peak located at 71.5 eV and Pt 4f 5/2 peak located at 74.8 eV correspond to metallic Pt(0), and the Pt 4f 7/2 peak located at 71.4 eV and Pt 4f 5/2 peak located at 74.9 eV correspond to Pt(II) in PtO or Pt(OH)₂. In addition, for the Pt₂CeO₂/CNTs-500 catalyst, the Pt 4f 7/2 peak located at 71.4 eV and Pt 4f 5/2 peak located at 74.9 eV correspond to metallic Pt(0), and the Pt 4f 7/2 peak located at 71.7 eV and Pt 4f 5/2 peak located at 75.5 eV correspond to Pt(II) in PtO or Pt(OH)₂. The fractions of the Pt(0) and Pt(II) species in Pt₂CeO₂/CNTs-300 and Pt₂CeO₂/CNTs-500 were calculated as (43.1%, 56.9%) and (41.8%, 58.2%), respectively. Obviously, the content of Pt(0) in Pt₂CeO₂/CNTs-400 is higher than Pt₂CeO₂/CNTs-300 and Pt₂CeO₂/CNTs-500, which shows 400 °C is the most favorable pyrolysis temperature for obtaining more Pt(0).

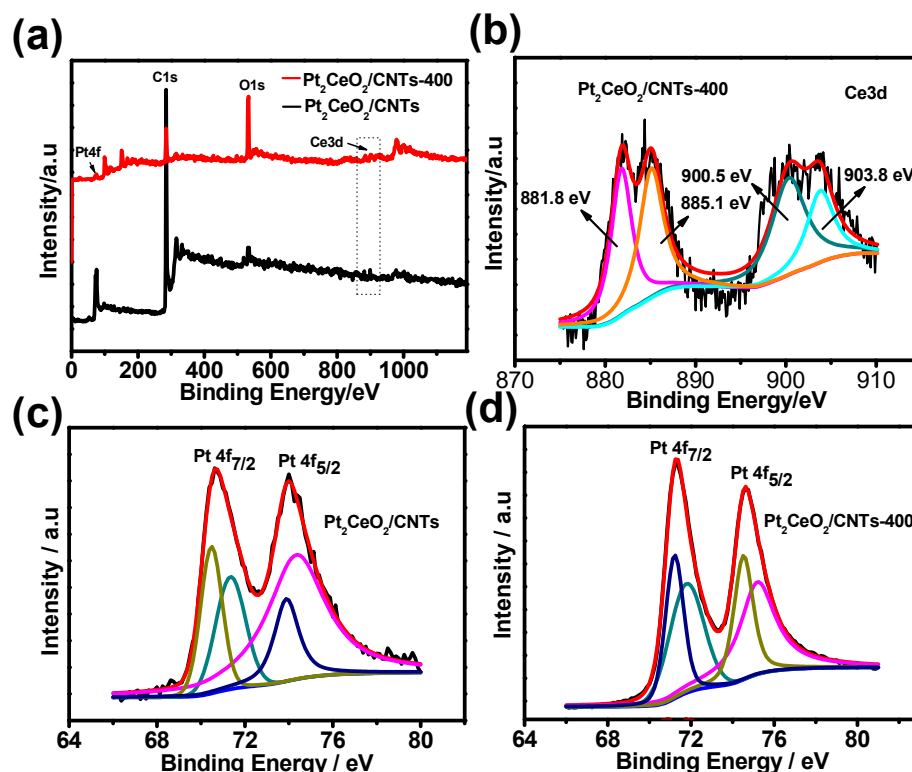


Figure 3. (a) XPS survey spectra, (b) Ce (3d) spectrum; Pt (3d) spectra of Pt₂CeO₂/CNTs (c), Pt₂CeO₂/CNTs-400 (d).

Figure 4a shows the CV of the Pt₂CeO₂/CNTs-400, Pt₂CeO₂/CNTs and Pt/C in 0.5 M H₂SO₄ solution at a scan rate of 50 mVs⁻¹. The hydrogen adsorption/desorption current peaks in the low potential region (−0.2~0.1 V) and the Pt oxidation/reduction current peaks in the high potential region (0.3~1.0 V) [38,48]. The electrochemical active

surface area (ECSA) was calculated by measuring the hydrogen adsorption/desorption charges after a double-layer correction and assuming a value of $210 \mu\text{C cm}^{-2}$ for the adsorption of a hydrogen monolayer [49]. Therefore, the ECSA of the $\text{Pt}_2\text{CeO}_2/\text{CNTs-400}$ was calculated to be $63.2 \text{ m}^2\text{g}^{-1}$, which is much higher than those of the $\text{Pt}_2\text{CeO}_2/\text{CNTs}$ ($41.7 \text{ m}^2\text{g}^{-1}$) and Pt/C ($21.3 \text{ m}^2\text{g}^{-1}$). The larger ECSA of $\text{Pt}_2\text{CeO}_2/\text{CNTs-400}$ is most likely due to the higher dispersion of Pt_2CeO_2 HJNS on the MWCNTs. In order to explore the effect of pyrolysis temperature on catalyst performance, we tested the catalytic performance of $\text{Pt}_2\text{CeO}_2/\text{CNTs-300}$, $\text{Pt}_2\text{CeO}_2/\text{CNTs-400}$ and $\text{Pt}_2\text{CeO}_2/\text{CNTs-500}$ for MOR (Figure 4b). For $\text{Pt}_2\text{CeO}_2/\text{CNTs-400}$, the peak current density in the forward scan is $839.1 \text{ mA mg}_{\text{Pt}}^{-1}$, higher than $\text{Pt}_2\text{CeO}_2/\text{CNTs-500}$ ($620.3 \text{ mA mg}_{\text{Pt}}^{-1}$) and $\text{Pt}_2\text{CeO}_2/\text{CNTs-300}$ ($459.2 \text{ mA mg}_{\text{Pt}}^{-1}$). The results show that the heat treatment of 400°C is more beneficial to the improvement of catalyst performance. Figure 4c shows the CV curves for MOR on the $\text{Pt}_2\text{CeO}_2/\text{CNTs-400}$, $\text{Pt}_2\text{CeO}_2/\text{CNTs}$ and Pt/C . For the $\text{Pt}_2\text{CeO}_2/\text{CNTs-400}$, the peak current density of MOR in the forward scans is much higher than those on the $\text{Pt}_2\text{CeO}_2/\text{CNTs}$ (641.6 mA mg^{-1}) and Pt/C (229.9 mA mg^{-1}). These results indicate that the electrocatalytic activity of $\text{Pt}_2\text{CeO}_2/\text{CNTs-400}$ for MOR is higher than $\text{Pt}_2\text{CeO}_2/\text{CNTs}$ and Pt/C . In order to further evaluate the long-term performance of $\text{Pt}_2\text{CeO}_2/\text{CNTs-400}$, $\text{Pt}_2\text{CeO}_2/\text{CNTs}$ and Pt/C , the CA were performed in $0.5 \text{ M CH}_3\text{OH} + 0.5 \text{ M H}_2\text{SO}_4$ solution at 0.5 V for 7200 s . As shown in Figure 4d, in the initial period, all of the curves with fast current decay indicate poisoning of the electrocatalysts due to the formation of intermediate species such as CO_{ads} [50]. After 7200 s , the $\text{Pt}_2\text{CeO}_2/\text{CNTs-400}$ catalyst maintained a higher current density ($23.2 \text{ mA mg}_{\text{Pt}}^{-1}$), which is almost 2.0 and 4.3 times those of the $\text{Pt}_2\text{CeO}_2/\text{CNTs}$ ($11.5 \text{ mA mg}_{\text{Pt}}^{-1}$) and Pt/C ($5.3 \text{ mA mg}_{\text{Pt}}^{-1}$), respectively. In order to further explore the multicycle CV stability of the catalysts, accelerated degradation tests (ADT) were conducted to check the durability of catalysts in $0.5 \text{ M H}_2\text{SO}_4 + 0.5 \text{ M CH}_3\text{OH}$ solution for 500 cycles (Figure S7 from Supplementary Materials). Obviously, the activity of the $\text{Pt}_2\text{CeO}_2/\text{CNTs-400}$ catalyst decreased rapidly (39.6%) during the first 200th cycle and decreased to 37.1% at the 400th cycle. By the 500th cycle, the activity had dropped to 35.0%. We can see that there is not much change in activity between the 400th and 500th cycles. However, the activity of $\text{Pt}_2\text{CeO}_2/\text{CNTs}$ and Pt/C catalysts still decreased significantly between the 400th and 500th cycles. After 500 cycles, the $\text{Pt}_2\text{CeO}_2/\text{CNTs-400}$ maintained a higher current density ($294.2 \text{ mA mg}_{\text{Pt}}^{-1}$) that is almost 2.6 and 4.9 times of the $\text{Pt}_2\text{CeO}_2/\text{CNTs}$ ($113.1 \text{ mA mg}_{\text{Pt}}^{-1}$) and Pt/C ($59.9 \text{ mA mg}_{\text{Pt}}^{-1}$), respectively. These results further illustrate that $\text{Pt}_2\text{CeO}_2/\text{CNTs-400}$ exhibits higher electrocatalytic stability for MOR. Besides, the $\text{Pt}_2\text{CeO}_2/\text{CNTs-400}$ catalyst presents the better MOR mass activity in comparison with the recent research works on Pt-based catalysts (Table S1 Supplementary Materials).

We used CO stripping experiments to investigate the CO tolerance of the as-prepared catalysts. Figure 5 shows the CO stripping voltammograms for the $\text{Pt}_2\text{CeO}_2/\text{CNTs-400}$, $\text{Pt}_2\text{CeO}_2/\text{CNTs}$ and Pt/C . Apparently, the onset potential of the adsorbed CO oxidation of the $\text{Pt}_2\text{CeO}_2/\text{CNTs-400}$ is negatively shifted to 0.47 V , and the corresponding potentials are 0.56 V and 0.58 V on the $\text{Pt}_2\text{CeO}_2/\text{CNTs}$ and Pt/C , respectively, indicating that thermal treatment effectively improves the CO oxidation ability of the catalyst [51,52].

The greatly enhanced electrocatalytic performance of the $\text{Pt}_2\text{CeO}_2/\text{CNTs-400}$ for the MOR may be due to four reasons: (1) the surface of CeO_2 coating contains more active sites of Pt deposition, and the Pt was dispersed more evenly, which reduced the surface energy; (2) the increased Lewis alkalinity of CeO_2 led to the strong anchoring of Pt to CeO_2 ; (3) the increase of Pt(0) composition during the carbonization of DES [47]; (4) the addition of appropriate CeO_2 , which changed the electronic state around the Pt atom, affected the adsorption of toxic intermediates. The addition of CeO_2 contributed to the uniform distribution of Pt and inhibited the agglomeration of Pt nanoparticles, but too much CeO_2 hindered the structure between Pt and CNTs, thus inhibiting the interaction between Pt, CeO_2 and CNTs. On the other hand, appropriate calcination temperature is conducive to the formation of fluorite structure of CeO_2 and the interaction between CeO_2 and CNTs, while higher calcination temperature may lead to CeO_2 agglomeration,

which is not conducive to the uniform distribution of Pt nanoparticles. In addition, higher calcination temperature may also lead to the collapse of CeO₂-CNTs structure and the reduction of surface area [53]. The mechanism of the advantages brought by the addition of DES and the influence of appropriate heat treatment on the catalyst are also under study.

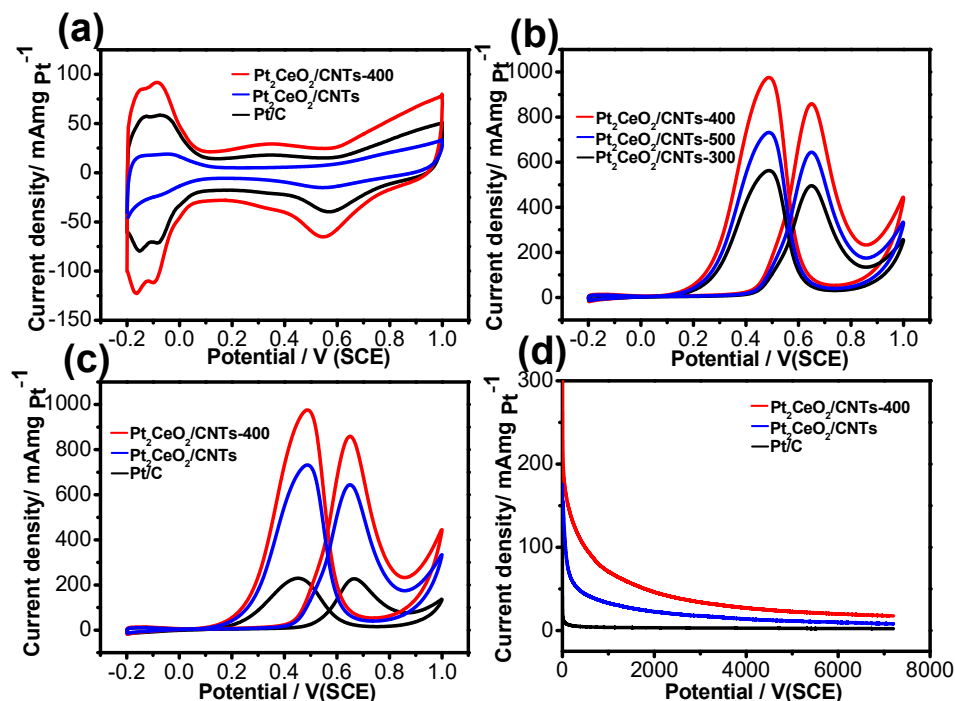


Figure 4. (a,c) Cyclic voltammograms and (d) current-time curves of Pt₂CeO₂/CNTs-400, Pt₂CeO₂/CNTs and Pt/C; (b) cyclic voltammogram curves of Pt₂CeO₂/CNTs-400, Pt₂CeO₂/CNTs and Pt/C in 0.5 M H₂SO₄/0.5 M CH₃OH+0.5 M H₂SO₄ solution.

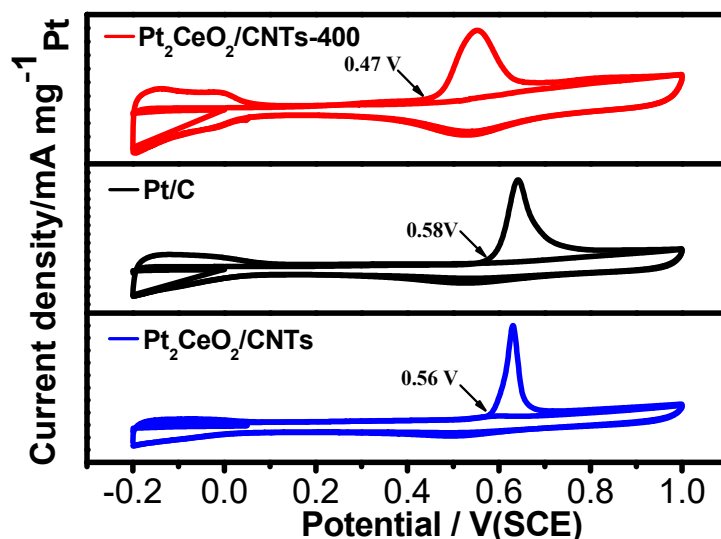


Figure 5. CO stripping voltammograms of Pt₂CeO₂/CNTs-400, Pt₂CeO₂/CNTs and Pt/C catalysts in 0.5 M H₂SO₄ solution.

3. Experimental Section

3.1. Materials

The raw MWCNTs (OD: 10–20 nm, Length: ~50 nm, Purity > 95 wt%) with 50 nm diameter, 10 mm length and 98% purity were bought from Shenzhen Nanotech Port Co. Ltd. Nafion solution (5 wt%) was purchased from Sigma-Aldrich. Urea (CO(NH₂)₂), choline

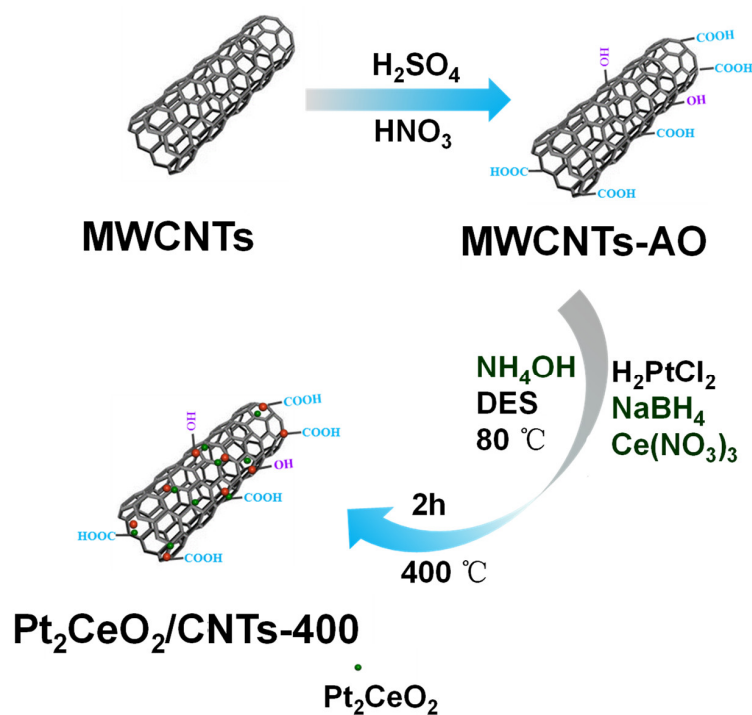
chloride [$\text{HOC}_2\text{H}_4\text{N}(\text{CH}_3)_3\text{Cl}$], chloroplatinic acid hexahydrate ($\text{H}_2\text{PtCl}_6 \cdot 6\text{H}_2\text{O}$), Cerium (III) nitrate hexahydrate ($\text{Ce}(\text{NO}_3)_3$), NH_4OH (ammonium hydroxide), Sodium borohydride (NaBH_4), Sulfuric acid (H_2SO_4), Nitric acid (HNO_3) and Ethanol ($\text{C}_2\text{H}_5\text{OH}$) were purchased from Shanghai Chemical Reagent Co. Ltd. All the chemicals were purchased at an analytical grade and utilized without further purification. All of the solutions were prepared with DESs.

3.2. Preparation of DES

DESs (choline chloride/urea) were prepared by a simple method according to the procedure in the reported literature [54]. Choline chloride [$\text{HOC}_2\text{H}_4\text{N}(\text{CH}_3)_3\text{Cl}$] (Shanghai Chemical Reagent Ltd., Shanghai, China 99%) was recrystallized from absolute ethanol, filtered and dried under vacuum. Urea (Shanghai Chemical Reagent Ltd., Shanghai, China >99%) was recrystallized from Millipore water (18.0 M Ω cm) provided by a Milli-Q Lab apparatus (Nihon Millipore Ltd., Tokyo, Japan), filtered and dried under vacuum prior to use. Briefly, urea and choline chloride with mole ratio of 2:1 were mixed and stirred at 80 °C until a homogeneous and colorless solution was formed. Then, the obtained DESs were preserved in a vacuum drying oven before use.

3.3. Preparation of Catalysts

Firstly, raw MWCNTs were treated with H_2SO_4 and HNO_3 to introduce surface oxygen groups and the samples collected after centrifugation were labelled as MWCNTs-AO [55]. Typically, a mixture containing appropriate ratios of $\text{H}_2\text{PtCl}_6 \cdot 6\text{H}_2\text{O}$, $\text{Ce}(\text{NO}_3)_3$ (atomic ratio: Pt/Ce = 1:0.5) and MWCNTs-AO was ultrasonicated until complete dispersion in DES (10 mL). Then, NaBH_4 (200 mg) and NH_4OH (5 mL) were added to this suspension and stirred continuously for 5 h at 80 °C. After stirring, the suspension was centrifuged and washed repeatedly with $\text{C}_2\text{H}_5\text{OH}$ and tri-distilled water. Later, it was dried at 60 °C for 24 h and the obtained product was labelled as $\text{Pt}_2\text{CeO}_2/\text{CNTs}$. Finally, $\text{Pt}_2\text{CeO}_2/\text{CNTs}$ were thermal treated at 300 °C, 400 °C and 500 °C in N_2 atmosphere for 2 h (refer to $\text{Pt}_2\text{CeO}_2/\text{CNTs}$ -300, $\text{Pt}_2\text{CeO}_2/\text{CNTs}$ -400 and $\text{Pt}_2\text{CeO}_2/\text{CNTs}$ -500). Scheme 1 shows the preparation of $\text{Pt}_2\text{CeO}_2/\text{CNTs}$ -400.



Scheme 1. Schematic illustration showing the preparation of $\text{Pt}_2\text{CeO}_2/\text{CNTs}$ -400.

3.4. Physical Characterization

The sizes, morphology and structure of all as-prepared nanocatalysts were characterized by X-ray diffraction (XRD), scanning electron microscopy (SEM), high-resolution transmission electron microscopy (HR-TEM), X-ray photoelectron spectroscopy (XPS) and (ICP-OES, Thermo Electron IRIS Intrepid II XSP, Waltham, MA, USA). XRD patterns were collected from a Rigaku D/max 2500Pc X-ray powder diffractometer (Rigaku D/MAX 2500 v/pc, Japan). SEM images were recorded using JSM-7500F electron microscopy. TEM and high-resolution TEM images were obtained with Talos F200S field emission electron microscope. The Pt contents in Pt/C, Pt₂CeO₂/CNTs and Pt₂CeO₂/CNTs-400 catalysts measured by ICP-OES were found to be 20.0, 19.3 and 17.7%, respectively.

3.5. Electrochemical Measurements

The catalyst-modified glassy carbon electrode (GC, diameter = 5 mm) was prepared based on a previously reported procedure [56]. An electrochemical workstation (Chenhua, Shanghai) was used to survey the electrochemical performances of prepared catalysts in a three-electrode system, where Pt foil and saturated calomel electrode served as the counter and reference electrodes, respectively. Earlier, GC electrode was polished with 5.0, 1.0 and 0.3 μm Al₂O₃ slurries and ultrasonically cleaned with ethanol and water. Then, catalyst (1.5 mg) was ultrasonically dispersed in Nafion solution (400 μL, 0.5 wt%), and the obtained mixture (10 μL) was slowly spun coated on the GC electrode at 25 °C. For Pt/C, Pt₂CeO₂/CNTs and Pt₂CeO₂/CNTs-400 catalysts, the corresponding Pt loadings on the GC electrode were 28.1, 26.4 and 25.2 μg cm⁻², respectively. The ECSA experiments were conducted in 0.5 M H₂SO₄ solution and the values were calculated by the integral area of hydrogen (H) adsorption/desorption peaks which appeared within the potential range of −0.2–0.35 V. The electrocatalytic activity of the prepared catalysts towards MOR was evaluated through cyclic voltammograms (CV) and chronoamperometric measurements (CA) in the electrolyte solution containing 0.5 M CH₃OH and 0.5 M H₂SO₄ at room temperature. For CO stripping voltammetry, CO was first passed through a 0.5 M H₂SO₄ solution for 15 min to achieve saturated CO absorption, while maintaining a voltage sweep from −0.2–0.0 V. Then, N₂ was passed through the electrolyte for 25 min to completely remove the dissolved CO while avoiding the interference of the O₂ in the air. All current values obtained in the electrochemical experiments were represented by normalized current per mg of Pt loading on the GC. Prior to each measurement, the electrolyte was purified with pure N₂ for 15 min, keeping the N₂ flow on the electrolyte to prevent the interference of the O₂. All the electrochemical results are presented as normalized current density (j mg_{Pt}⁻¹).

4. Conclusions

A simple and effective chemical reduction approach has been developed for the fabrication of Pt₂CeO₂/CNTs-400 with the help of DES and thermal treatment. The catalyst exhibited an enhanced electrocatalytic performance (higher activity, long-term durability and excellent CO tolerance) compared to the Pt₂CeO₂/CNTs and Pt/C. This study demonstrates the DES medium and CeO₂ coating in favor of a uniform distribution for Pt nanoparticles on the carbon support. The improved performance of Pt₂CeO₂/CNTs-400 is attributed to the addition of appropriate CeO₂, which changed the electronic state around the Pt atom, formed new Ce-O-Pt bond at the interface between Pt and CeO₂ acting as new active sites, affected the adsorption of toxic intermediates and weakened the dissolution of Pt; on the other hand, with the assistance of thermal treatment, the DES is beneficial to the increase of the effective component Pt(0) in the carbonization process to enhance the dehydrogenation process of MOR.

Supplementary Materials: The following supporting information can be downloaded at: <https://www.mdpi.com/article/10.3390/molecules28072995/s1>. Figure S1. XRD patterns of Pt₂CeO₂/CNTs-300 and Pt₂CeO₂/CNTs-500 catalysts; Figure S2. TEM and HRTEM images of Pt₂CeO₂/CNTs; Figure S3. TEM and HRTEM images of Pt₂CeO₂/CNTs-300 (a,b) and Pt₂CeO₂/CNTs-500 (c,d)

catalysts; Figure S4. EDS of Pt₂CeO₂/CNTs-400; Figure S5. Ce3d spectra (locally enlarged) of Pt₂CeO₂/CNTs-400 and Pt₂CeO₂/CNTs; Figure S6. XPS survey spectra, Ce (3d) spectrum; Pt (3d) spectrum of Pt₂CeO₂/CNTs-300, Pt₂CeO₂/CNTs-500; Figure S7. accelerated degradation tests (ADT) CV curves of Pt₂CeO₂/CNTs-400 (a), Pt₂CeO₂/CNTs (b), Pt/C (c) catalysts in 0.5 M H₂SO₄ + 0.5 M CH₃OH solution (100th, 200th, 400th and 500th cycles); Table S1. A recent literatures survey of the activity (mA mg⁻¹ Pt) of MOR electrocatalysts. References [57–68] are provided from Supplementary Materials.

Author Contributions: Conceptualization, P.Y.; methodology, L.Z.; software, L.Z.; validation, S.D.; formal analysis, S.D.; investigation, S.D.; resources, W.C.; data curation, D.M.; writing—original draft preparation, P.Y.; writing—review and editing, P.Y.; visualization, X.W.; supervision, X.W.; project administration, Y.O.; funding acquisition, Y.O. All authors have read and agreed to the published version of the manuscript.

Funding: This research was funded by the Key Project of Hunan Provincial Education Department of China (22A0551), the Natural Science Foundation of Hunan Province (2020JJ4073), Hunan Provincial general project of Education Department (21C0645). Key project of Huaihua University (HHUY2021-03).

Institutional Review Board Statement: Not applicable.

Informed Consent Statement: Not applicable.

Data Availability Statement: Data are available on request; please contact P.Y., yangpingping0218@163.com.

Acknowledgments: The authors thank the Key Project of Hunan Provincial Education Department of China (22A0551), the Natural Science Foundation of Hunan Province (2020JJ4073), Hunan Provincial general project of Education Department (21C0645). Key project of Huaihua University (HHUY2021-03).

Conflicts of Interest: The authors declare no conflict of interest.

References

1. Zhang, W.; Yang, Y.; Huang, B.; Lv, F.; Wang, K.; Li, N.; Luo, M.; Chao, Y.; Li, Y.; Sun, Y.; et al. Ultrathin PtNiM (M = Rh, Os, and Ir) Nanowires as Efficient Fuel Oxidation Electrocatalytic Materials. *Adv. Mater.* **2019**, *31*, e1805833. [CrossRef] [PubMed]
2. Bu, L.; Shao, Q.; Bin, E.; Guo, J.; Yao, J.; Huang, X. PtPb/PtNi Intermetallic Core/Atomic Layer Shell Octahedra for Efficient Oxygen Reduction Electrocatalysis. *J. Am. Chem. Soc.* **2017**, *139*, 9576–9582. [CrossRef] [PubMed]
3. Jiang, Z.; Song, S.; Zheng, X.; Liang, X.; Li, Z.; Gu, H.; Li, Z.; Wang, Y.; Liu, S.; Chen, W.; et al. Lattice Strain and Schottky Junction Dual Regulation Boosts Ultrafine Ruthenium Nanoparticles Anchored on a N-Modified Carbon Catalyst for H₂ Production. *J. Am. Chem. Soc.* **2022**, *144*, 19619–19626. [CrossRef] [PubMed]
4. Yang, P.; Yang, X.; Liu, W.; Guo, R.; Yao, Z. Graphene-based electrocatalysts for advanced energy conversion. *Green Energy Environ.* **2022**, *in press*. [CrossRef]
5. Bai, G.; Liu, C.; Gao, Z.; Lu, B.; Tong, X.; Guo, X.; Yang, N. Atomic Carbon Layers Supported Pt Nanoparticles for Minimized CO Poisoning and Maximized Methanol Oxidation. *Small* **2019**, *15*, 1902951. [CrossRef]
6. Luo, B.; Zhao, F.; Xie, Z.; Yuan, Q.; Yang, F.; Yang, X.; Li, C.; Zhou, Z. Polyhedron-Assembled Ternary PtCuCo Nanochains: Integrated Functions Enhance the Electrocatalytic Performance of Methanol Oxidation at Elevated Temperature. *ACS Appl. Mater. Interfaces* **2019**, *11*, 32282–32290. [CrossRef]
7. Yang, X.; Liang, Z.; Chen, S.; Ma, M.; Wang, Q.; Tong, X.; Zhang, Q.; Ye, J.; Gu, L.; Yang, N. A Phosphorus-Doped Ag@Pd Catalyst for Enhanced C-C Bond Cleavage during Ethanol Electrooxidation. *Small* **2020**, *16*, e2004727. [CrossRef]
8. Zhang, L.Y.; Gong, Y.; Wu, D.; Wu, G.; Xu, B.; Bi, L.; Yuan, W.; Cui, Z. Twisted palladium-copper nanochains toward efficient electrocatalytic oxidation of formic acid. *J. Colloid Interface Sci.* **2019**, *537*, 366–374. [CrossRef]
9. Touni, A.; Liu, X.; Kang, X.; Papoulia, C.; Pavlidou, E.; Lambropoulou, D.; Tsampas, M.N.; Chatzitakis, A.; Sotiropoulos, S. Methanol Oxidation at Platinum Coated Black Titania Nanotubes and Titanium Felt Electrodes. *Molecules* **2022**, *27*, 6382. [CrossRef]
10. Hurley, N.; Li, L.; Koenigsmann, C.; Wong, S.S. Surfactant-Free Synthesis of Three-Dimensional Perovskite Titania-Based Micron-Scale Motifs Used as Catalytic Supports for the Methanol Oxidation Reaction. *Molecules* **2021**, *26*, 909. [CrossRef]
11. Dao, D.V.; Le, T.D.; Adilbish, G.; Lee, I.H.; Yu, Y.T. Pt-loaded Au@CeO₂ core-shell nanocatalysts for improving methanol oxidation reaction activity. *J. Mater. Chem. A* **2019**, *7*, 26996–27006. [CrossRef]
12. Lin, Z.; Chen, W.; Jiang, Y.; Bian, T.; Zhang, H.; Wu, J.; Wang, Y.; Yang, D. Facile synthesis of Ru-decorated Pt cubes and icosahedra as highly active electrocatalysts for methanol oxidation. *Nanoscale* **2016**, *8*, 12812–12818. [CrossRef] [PubMed]
13. Yang, J.; Tan, X.; Qian, Y.; Li, L.; Xue, Y.; Dai, Z.; Wang, H.; Qu, W.; Chu, Y. Methanol oxidation on Pt-CeO₂@C-N electrocatalysts prepared by the in-situ carbonization of polyvinylpyrrolidone. *J. Appl. Electrochem.* **2016**, *46*, 779–789. [CrossRef]
14. Tao, L.; Shi, Y.; Huang, Y.C.; Chen, R.; Zhang, Y.; Huo, J.; Zou, Y.; Yu, G.; Luo, J.; Dong, C.L.; et al. Interface engineering of Pt and CeO₂ nanorods with unique interaction for methanol oxidation. *Nano Energy* **2018**, *53*, 604–612. [CrossRef]

15. Feng, Y.Y.; Hu, H.S.; Song, G.H.; Si, S.; Liu, R.J.; Peng, D.-N.; Kong, D.-S. Promotion effects of CeO₂ with different morphologies to Pt catalyst toward methanol electrooxidation reaction. *J. Alloys Compd.* **2019**, *798*, 706–713. [[CrossRef](#)]
16. Zou, L.; Pan, J.; Xu, F.; Chen, J. Cu assisted loading of Pt on CeO₂ as a carbon-free catalyst for methanol and oxygen reduction reaction. *RSC Adv.* **2021**, *11*, 36726–36733. [[CrossRef](#)]
17. Teng, Z.; Zhang, Z.; Li, X. Preparation of Pt catalysts supported on polyaniline modified carbon black and electrocatalytic methanol oxidation. *Synth. Met.* **2023**, *293*, 117256. [[CrossRef](#)]
18. Zhou, W.; Du, Y.; Ren, F.; Wang, C.; Xu, J.; Yang, P. High efficient electrocatalytic oxidation of methanol on Pt/polyindoles composite catalysts. *Inter. J. Hydrogen Energy* **2010**, *35*, 3270–3279. [[CrossRef](#)]
19. Muhmood, T.; Xia, M.; Lei, W.; Wang, F.; Mahmood, A. Fe-ZrO₂ imbedded graphene like carbon nitride for acarbose (ACB) photo-degradation intermediate study. *Adv. Powder Technol.* **2018**, *29*, 3233–3240. [[CrossRef](#)]
20. Yang, P.P.; Zhao, P.C.; Luo, N.; Li, Y.H.; Wang, C.; Zhang, L.; Xie, Y.X.; Fei, J.J. A “special” anhydrous system for the preparation of alloyed Pd₁Ce_{0.5} nanonetworks catalyst supported on carbon nanotubes with high electrochemical oxidation activity for formic acid. *Inter. J. Hydrogen Energy* **2021**, *46*, 18857–18865. [[CrossRef](#)]
21. Yang, P.; Zhou, Z.; Zheng, T.; Gu, C.; Gong, X.; Zhang, Y.; Xie, Y.; Yang, N.; Fei, J. A novel strategy to synthesize Pt/CNTs nanocatalyst with highly improved activity for methanol electrooxidation. *J. Electroanal. Chem.* **2021**, *897*, 115557. [[CrossRef](#)]
22. Li, Y.; Tang, J.; Lin, Y.; Li, J.; Yang, Y.; Zhao, P.; Fei, J.; Xie, Y. Ultrasensitive Determination of Natural Flavonoid Rutin Using an Electrochemical Sensor Based on Metal-Organic Framework CAU-1/Acidified Carbon Nanotubes Composites. *Molecules* **2022**, *27*, 7761. [[CrossRef](#)] [[PubMed](#)]
23. Mahmood, A.; Muhmood, T.; Ahmad, F. Carbon nanotubes heterojunction with graphene like carbon nitride for the enhancement of electrochemical and photocatalytic activity. *Mate. Chem. Phys.* **2022**, *278*, 125640. [[CrossRef](#)]
24. Yang, P.; Devasenathipathy, R.; Xu, W.; Wang, Z.; Chen, D.-H.; Zhang, X.; Fan, Y.; Chen, W. Pt₁(CeO₂)_{0.5} Nanoparticles Supported on Multiwalled Carbon Nanotubes for Methanol Electro-oxidation. *ACS Appl. Nano Mater.* **2021**, *4*, 10584–10591. [[CrossRef](#)]
25. Yu, T.; Xu, Q.; Luo, L.; Liu, C.; Yin, S. Interface engineering of NiO/RuO₂ heterojunction nano-sheets for robust overall water splitting at large current density. *Chem. Eng. J.* **2022**, *430*, 133117. [[CrossRef](#)]
26. Muhmood, T.; Xia, M.; Lei, W.; Wang, F. Under vacuum synthesis of type-I heterojunction between red phosphorus and graphene like carbon nitride with enhanced catalytic, electrochemical and charge separation ability for photodegradation of an acute toxicity category-III compound. *Appl. Catal. B Environ.* **2018**, *238*, 568–575. [[CrossRef](#)]
27. Muhmood, T.; Xia, M.; Lei, W.; Wang, F.; Khan, M.A. Design of Graphene Nanoplatelet/Graphitic Carbon Nitride Heterojunctions by Vacuum Tube with Enhanced Photocatalytic and Electrochemical Response. *Eur. J. Inorg. Chem.* **2018**, *2018*, 1726–1732. [[CrossRef](#)]
28. Wagle, D.V.; Zhao, H.; Baker, G.A. Deep eutectic solvents: Sustainable media for nanoscale and functional materials. *Acc. Chem. Res.* **2014**, *47*, 2299–2308. [[CrossRef](#)]
29. Wei, L.; Mao, Y.; Liu, F.; Sheng, T.; Wei, Y.; Li, J.; Fan, Y.J. Concave Cubic Pt–Sm Alloy Nanocrystals with High-Index Facets and Enhanced Electrocatalytic Ethanol Oxidation. *ACS Appl. Energy Mater.* **2019**, *2*, 7204–7210. [[CrossRef](#)]
30. Wei, L.; Fan, Y.J.; Tian, N.; Zhou, Z.Y.; Zhao, X.Q.; Mao, B.W.; Sun, S.G. Electrochemically Shape-Controlled Synthesis in Deep Eutectic Solvents—A New Route to Prepare Pt Nanocrystals Enclosed by High-Index Facets with High Catalytic Activity. *J. Phys. Chem. C* **2011**, *116*, 2040–2044. [[CrossRef](#)]
31. Wei, L.; Zhou, Z.Y.; Chen, S.P.; Xu, C.D.; Su, D.; Schuster, M.E.; Sun, S.G. Electrochemically shape-controlled synthesis in deep eutectic solvents: Triambic icosahedral platinum nanocrystals with high-index facets and their enhanced catalytic activity. *Chem. Commun.* **2013**, *49*, 11152–11154. [[CrossRef](#)] [[PubMed](#)]
32. Wei, L.; Fan, Y.J.; Wang, H.H.; Tian, N.; Zhou, Z.Y.; Sun, S.G. Electrochemically shape-controlled synthesis in deep eutectic solvents of Pt nanoflowers with enhanced activity for ethanol oxidation. *Electrochim. Acta* **2012**, *76*, 468–474. [[CrossRef](#)]
33. Abbott, A.P.; Capper, G.; Davies, D.L.; Rasheed, R.K.; Tambyrajah, V. Novel solvent properties of choline chloride/urea mixtures. *Chem. Commun.* **2003**, *39*, 70–71. [[CrossRef](#)] [[PubMed](#)]
34. Liao, H.G.; Jiang, Y.X.; Zhou, Z.Y.; Chen, S.P.; Sun, S.G. Shape-controlled synthesis of gold nanoparticles in deep eutectic solvents for studies of structure-functionality relationships in electrocatalysis. *Angew. Chem. Int. Ed. Engl.* **2008**, *47*, 9100–9103. [[CrossRef](#)] [[PubMed](#)]
35. Abbott, A.P.; Boothby, D.; Capper, G.; Davies, D.L.; Rasheed, R.K. Deep Eutectic Solvents Formed between Choline Chloride and Carboxylic Acids: Versatile Alternatives to Ionic Liquids. *J. Am. Chem. Soc.* **2004**, *126*, 9142–9147. [[CrossRef](#)] [[PubMed](#)]
36. Liao, C.H.; Chen, J.Y.; Liu, G.Y.; Xu, Z.R.; Lee, S.; Chiang, C.K.; Hsieh, Y.T. Supercritical Fluid-Assisted Fabrication of Pd Nanoparticles/Graphene Using a Choline Chloride-Oxalic Acid Deep Eutectic Solvent for Enhancing the Electrochemical Oxidation of Glycerol. *ACS Omega* **2022**, *7*, 19930–19938. [[CrossRef](#)]
37. Juárez-Marmolejo, L.; Maldonado-Teodocio, B.; de Oca-Yemha, M.G.M.; Romero-Romo, M.; Ramírez-Silva, M.T.; Arce-Estrada, E.M.; Morales-Gil, P.; Mostany, J.; Palomar-Pardavé, M. Electrochemical Deposition of Pd@Pd(OH)₂ Core-Shell Nanoparticles onto Glassy Carbon from a Deep Eutectic Solvent (Reline) and their Use as Electrocatalyst for the Methanol Oxidation Reaction. *J. Electrochem. Soc.* **2020**, *167*, 112509. [[CrossRef](#)]
38. Zhong, J.; Li, L.; Waqas, M.; Wang, X.; Fan, Y.; Qi, J.; Yang, B.; Rong, C.; Chen, W.; Sun, S. Deep eutectic solvent-assisted synthesis of highly efficient PtCu alloy nanoclusters on carbon nanotubes for methanol oxidation reaction. *Electrochim. Acta* **2019**, *322*, 134677. [[CrossRef](#)]

39. Xiang, S.; Wang, L.; Huang, C.C.; Fan, Y.-J.; Tang, H.G.; Wei, L.; Sun, S.G. Concave cubic PtLa alloy nanocrystals with high-index facets: Controllable synthesis in deep eutectic solvents and their superior electrocatalytic properties for ethanol oxidation. *J. Power Sources* **2018**, *399*, 422–428. [[CrossRef](#)]
40. Yang, P.; Li, Y.; Chen, S.; Li, J.; Zhao, P.; Zhang, L.; Xie, Y.; Fei, J. One-step synthesis in deep eutectic solvents of Pt₃Sn₁-SnO₂ alloy nanopore on carbon nanotubes for boosting electro-catalytic methanol oxidation. *J. Electroanal. Chem.* **2021**, *887*, 115164. [[CrossRef](#)]
41. Yang, P.; Wei, L.; Xiao, X.; Zhou, Z.; Li, J.; Zhang, Y.; Xie, Y.; Yang, N.; Fei, J. Electrocatalytic oxidation of formic acid on Pd/CNTs nanocatalysts synthesized in special “non-aqueous” system. *J. Electroanal. Chem.* **2022**, *906*, 115980. [[CrossRef](#)]
42. Zhang, J.M.; Wang, R.X.; Nong, R.J.; Li, Y.; Zhang, X.J.; Zhang, P.Y.; Fan, Y.J. Hydrogen co-reduction synthesis of PdPtNi alloy nanoparticles on carbon nanotubes as enhanced catalyst for formic acid electrooxidation. *Inter. J. Hydrogen Energy* **2017**, *42*, 7226–7234. [[CrossRef](#)]
43. Li, Y.H.; Deng, H.C.; Zhou, Z.H.; Yang, P.P.; Fei, J.J.; Xie, Y.X. Pd₁₂Ag₁ nanoalloy on dendritic CNFs catalyst for boosting formic acid oxidation. *Appl. Surf. Sci.* **2023**, *608*, 155131. [[CrossRef](#)]
44. Wei, L.; Fan, Y.J.; Ma, J.H.; Tao, L.H.; Wang, R.X.; Zhong, J.P.; Wang, H. Highly dispersed Pt nanoparticles supported on manganese oxide-poly (3,4-ethylenedioxythiophene)-carbon nanotubes composite for enhanced methanol electrooxidation. *J. Power Sources* **2013**, *238*, 157–164. [[CrossRef](#)]
45. Zhong, J.; Sun, M.; Xiang, S.; Fan, Y.; Waqas, M.; Huang, K.; Tang, Y.; Chen, W.; Yang, J. Sulfonated cobalt phthalocyanine-derived Co-N-S tridoped carbon nanotubes as platinum catalyst supports for highly efficient methanol electrooxidation. *Appl. Surf. Sci.* **2020**, *511*, 145519. [[CrossRef](#)]
46. Zhong, J.P.; Fan, Y.J.; Wang, H.; Wang, R.X.; Fan, L.L.; Shen, X.C.; Shi, Z.J. Copper phthalocyanine functionalization of graphene nanosheets as support for platinum nanoparticles and their enhanced performance toward methanol oxidation. *J. Power Sources* **2013**, *242*, 208–215. [[CrossRef](#)]
47. Chu, Y.Y.; Cao, J.; Dai, Z.; Tan, X.Y. A novel Pt/CeO₂ catalyst coated with nitrogen-doped carbon with excellent performance for DMFCs. *J. Mater. Chem. A* **2014**, *2*, 4038–4044. [[CrossRef](#)]
48. Zhang, J.M.; He, J.J.; Wang, X.Q.; Fan, Y.J.; Zhang, X.J.; Zhong, J.P.; Chen, W.; Sun, S.G. One-step synthesis in deep eutectic solvents of PtV alloy nanonetworks on carbon nanotubes with enhanced methanol electrooxidation performance. *Int. J. Hydrogen Energy* **2019**, *44*, 28709–28719. [[CrossRef](#)]
49. Li, Y.; Gao, W.; Ci, L.; Wang, C.; Ajayan, P.M. Catalytic performance of Pt nanoparticles on reduced graphene oxide for methanol electro-oxidation. *Carbon* **2010**, *48*, 1124–1130. [[CrossRef](#)]
50. Zhang, L.Y.; Gong, Y.; Liu, H.; Yuan, W.; Liu, Z. Ultrasmall and uniform Pt₃Au clusters strongly suppress Ostwald ripening for efficient ethanol oxidation. *Electrochem. Commun.* **2017**, *84*, 1–5. [[CrossRef](#)]
51. Zeng, T.; Meng, X.; Huang, H.; Zheng, L.; Chen, H.; Zhang, Y.; Yuan, W.; Zhang, L.Y. Controllable Synthesis of Web-Footed PdCu Nanosheets and Their Electrocatalytic Applications. *Small* **2022**, *18*, e2107623. [[CrossRef](#)] [[PubMed](#)]
52. Wang, S.; Wang, F.; Liu, H.; Huang, H.; Meng, X.; Ouyang, Y.; Jiang, M.; Zeng, T.; Chen, H.; Zheng, L.; et al. Defective PdRh bimetallic nanocrystals enable enhanced methanol electrooxidation. *Colloids Surf. A* **2021**, *616*, 126323. [[CrossRef](#)]
53. Yang, J.; Chu, Y.; Li, L.; Wang, H.; Dai, Z.; Tan, X.Y. Effects of calcination temperature and CeO₂ contents on the performance of Pt/CeO₂-CNTs hybrid nanotube catalysts for methanol oxidation. *J. Appl. Electrochem.* **2016**, *46*, 369–377. [[CrossRef](#)]
54. Wei, L.; Xu, C.D.; Huang, L.; Zhou, Z.Y.; Chen, S.P.; Sun, S.G. Electrochemically Shape-Controlled Synthesis of Pd Concave-Disdyakis Triacantahedra in Deep Eutectic Solvent. *J. Phys. Chem. C* **2015**, *120*, 15569–15577. [[CrossRef](#)]
55. Yang, P.; Zhang, L.; Wei, X.; Dong, S.; Ouyang, Y. Pd₍₃₎Co₍₁₎ Alloy Nanocluster on the MWCNT Catalyst for Efficient Formic Acid Electro-Oxidation. *Nanomaterials* **2022**, *12*, 4182. [[CrossRef](#)] [[PubMed](#)]
56. Yang, P.; Zhang, L.; Wei, X.; Dong, S.; Cao, W.; Ma, D.; Ouyang, Y.; Xie, Y.; Fei, J. A “Special” Solvent to Prepare Alloyed Pd₍₂₎Ni₍₁₎ Nanoclusters on a MWCNT Catalyst for Enhanced Electrocatalytic Oxidation of Formic Acid. *Nanomaterials* **2023**, *13*, 755. [[CrossRef](#)]
57. Xu, H.; Wang, A.L.; Tong, Y.X.; Li, G.-R. Enhanced Catalytic Activity and Stability of Pt/CeO₂/PANI Hybrid Hollow Nanorod Arrays for Methanol Electro-oxidation. *ACS Catal.* **2016**, *6*, 5198–5206. [[CrossRef](#)]
58. Zhao, L.; Sui, X.L.; Li, J.Z.; Zhang, J.J.; Zhang, L.M.; Huang, G.S.; Wang, Z.B. Supramolecular assembly promoted synthesis of three-dimensional nitrogen doped graphene frameworks as efficient electrocatalyst for oxygen reduction reaction and methanol electrooxidation. *Appl. Catal. B Environ.* **2018**, *231*, 224–233. [[CrossRef](#)]
59. Wang, R.X.; Fan, J.J.; Fan, Y.J.; Zhong, J.P.; Wang, L.; Sun, S.G.; Shen, X.C. Platinum nanoparticles on porphyrin functionalized graphene nanosheets as a superior catalyst for methanol electrooxidation. *Nanoscale* **2014**, *6*, 14999–15007. [[CrossRef](#)]
60. Zhang, J.-M.; Sun, S.-N.; Li, Y.; Zhang, X.-J.; Zhang, P.-Y.; Fan, Y.-J. A strategy in deep eutectic solvents for carbon nanotube-supported PtCo nanocatalysts with enhanced performance toward methanol electrooxidation. *Int. J. Hydrogen Energy* **2017**, *42*, 26744–26751. [[CrossRef](#)]
61. Wang, X.; Sun, M.; Xiang, S.; Waqas, M.; Fan, Y.; Zhong, J.; Huang, K.; Chen, W.; Liu, L.; Yang, J. Template-free synthesis of platinum hollow-opened structures in deep-eutectic solvents and their enhanced performance for methanol electrooxidation. *Electrochim. Acta* **2020**, *337*, 135742. [[CrossRef](#)]
62. Yang, B.; Huang, K.; Hu, S.; Wang, R.; Fan, Y.; Qi, J.; Rong, C.; Zeng, J.; Chen, W. Platinum nanoparticles anchored on aminated silica@PEDOT-PSS hybrid for enhanced methanol oxidation electrocatalysis. *Int. J. Hydrogen Energy* **2020**, *45*, 30473–30483. [[CrossRef](#)]

63. Fan, J.J.; Fan, Y.J.; Wang, R.X.; Xiang, S.; Tang, H.G.; Sun, S.G. A novel strategy for the synthesis of sulfur-doped carbon nanotubes as a highly efficient Pt catalyst support toward the methanol oxidation reaction. *J. Mater Chem. A* **2017**, *5*, 19467–19475. [[CrossRef](#)]
64. Huang, K.; Zhong, J.; Huang, J.; Tang, H.; Fan, Y.; Waqas, M.; Yang, B.; Chen, W.; Yang, J. Fine platinum nanoparticles supported on polyindole-derived nitrogen-doped carbon nanotubes for efficiently catalyzing methanol electrooxidation. *Appl. Surf. Sci.* **2020**, *501*, 144260. [[CrossRef](#)]
65. Yang, F.; Yang, B.; Rani, K.K.; Wei, Y.; Peng, X.; Wang, L.; Liu, X.; Chen, D.-H.; Fan, Y.; Chen, W. Revealing the role of Ni²⁺ ions in inducing the synthesis of porous carbon balls: A novel substrate to enhance the Pt catalytic activity towards methanol-oxidation. *Int. J. Hydrogen Energy* **2022**, *47*, 23583–23592. [[CrossRef](#)]
66. Wang, P.; Zhang, Y.; Shi, R.; Wang, Z. Trimetallic PtPdCu nanowires as an electrocatalyst for methanol and formic acid oxidation. *New J. Chem.* **2018**, *42*, 19083–19089. [[CrossRef](#)]
67. Zhang, Y.; Shi, R.; Ren, J.; Dai, Y.; Yuan, Y.; Wang, Z. PtFeCu Concave Octahedron Nanocrystals as Electrocatalysts for the Methanol Oxidation Reaction. *Langmuir* **2019**, *35*, 16752–16760. [[CrossRef](#)]
68. Wang, P.; Zhang, Y.; Shi, R.; Wang, Z. Shape-Controlled Synthesis of Trimetallic PtPdCu Nanocrystals and Their Electrocatalytic Properties. *ACS Appl. Energy Mater.* **2019**, *2*, 2515–2523. [[CrossRef](#)]

Disclaimer/Publisher’s Note: The statements, opinions and data contained in all publications are solely those of the individual author(s) and contributor(s) and not of MDPI and/or the editor(s). MDPI and/or the editor(s) disclaim responsibility for any injury to people or property resulting from any ideas, methods, instructions or products referred to in the content.